L-band x-ray absorption of radiatively heated nickel

C. Chenais-Popovics, M. Fajardo,* F. Gilleron, U. Teubner,† and J.-C. Gauthier
Laboratoire pour l'Utilisation des Lasers Intenses, UMR 7605 CNRS, Ecole Polytechnique, 91128 Palaiseau Cedex, France

C. Bauche-Arnoult, A. Bachelier, and J. Bauche
Laboratoire Aimé Cotton, Bâtiment 505, Campus d'Orsay, 91405 Orsay Cedex, France

T. Blenski and F. Thais
CEA Saclay, DSM/DRECAM/SPAM, 91191 Gif-Sur-Yvette Cedex, France

F. Perrot
CEA/DAM, Boîte Postale 12, 91680 Bruyères-le-Châtel, France

A. Benuzzi, S. Turck-Chièze, and J.-P. Chièze
CEA Saclay, DSM/DAPNIA/SAp, 91191 Gif-Sur-Yvette Cedex, France

F. Dorchies
INRS Energie, Varennes, Québec, Canada

U. Andiel, W. Foelsner, and K. Eidmann
Max-Planck Institut für Quantenoptik, D-85740 Garching, Germany

(Received 18 January 2001; revised manuscript received 8 October 2001; published 19 December 2001)

Absorption of *L-M* and *L-N* transitions of nickel has been measured using point projection spectroscopy. The x-ray radiation from laser-irradiated gold cavities was used to heat volumetrically nickel foils ''tamped with carbon'' up to 20 eV. Experimental spectra have been analyzed with calculations based on the spin-orbit split arrays statistical approach and performed for each ionic species Ni^{5+} to Ni^{11+}. Using a least-squares fit, this method provides an ion distribution broader than at local thermodynamic equilibrium, which is explained by spatial and temporal temperature gradients. A major improvement in the simulation of the absolute value of transmission is obtained with a resolved transition array statistical calculation that reproduces the experimental spectrum with the nominal areal mass density by taking into account the saturation of narrow lines.

DOI: 10.1103/PhysRevE.65.016413 PACS number(s): 52.25.Os, 52.50.Jm, 95.30.Jx, 97.10.Ex

I. INTRODUCTION

Radiative properties of stars and inertial confinement fusion plasmas are governed by the absorption coefficients of matter heated in hot plasma conditions. Even if the composition of stars is dominated by hydrogen and helium, a small percentage of medium-*Z* elements, e.g., iron and elements of near atomic numbers, is ruling the radiative transfer because their absorption coefficients are large [1]. Earlier measurements of the $3p$-$3d$ iron transitions [2], and their analysis with the opacity code OPAL [3] including $\Delta n=0$ transitions have been a real improvement for the cepheid pulsation description [4,5]. More recently, the measurement of the $2p$-$3d$ iron structure around Fe VIII [6] has been used to identify a similar iron absorption structure in the quasar IRAS 13349 +2438 spectrum recorded by the XMM Newton satellite [7].

Several measurements of absorption coefficients have pointed out the importance of the quality of the sample foils for a reliable measurement of the absolute transmission of the foil [6,8,9], in particular, for the agreement of theories with the absolute value of the measured transmission. This led us to carry a systematic study of the absorption of *L-M* and *L-N* transitions ($n=2$ to $n=3$ and 4) of nickel samples, as this element has a number of bound electrons close to iron and may be obtained in homogeneous thin foils. In the present experiment, we investigate a regime of low temperatures, in which the opacity codes have not been much tested versus experimental data. Our goal here is to compare experimental data to codes based on the unresolved transition array (UTA) formalism [10] in which the different level-to-level transitions are not treated individually, and to discuss their possibilities and limits. The UTA method has proven to reproduce very accurately absorption spectra, in comparison with a number of experiments, especially at high density, when the lines are broad and overlap [11,12]. Calculations were performed here for individual ions with the spin-orbit-split arrays (SOSA) approach that is a UTA description in which arrays are divided in separate subarrays due to large spin-orbit interactions [13,14]. This model permits one to determine the ionic fractions by a fine adjustment of the experimental spectra, without the assumption that the ionic

*Also with Grupo de Lasers e Plasmas, Instituto Superior Técnico, 1 Avenida Rovisco Pais, Lisboa, Portugal.

†Permanent address: Institut für Optik und Quantenelektronik, Friedrich-Schiller-Universität Jena, Max-Wien-Platz 1, D-07743 Jena, Germany.

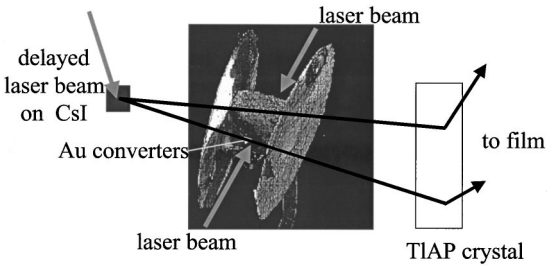

FIG. 1. Schematic experimental mounting. The heating cavity is a 1 mm long cylinder of 1 mm diameter. Two 3 mm diameter gold flanges protect the line of sight from the emission at the front of the gold foil.

distribution is in local thermodynamic equilibrium (LTE). A number of experiments analyzed with methods based on the UTA formalism show a discrepancy in the absolute value of the measured absorption versus theory: the experimental absorption is weaker than the calculated value obtained for the areal density given by the manufacturer [6,8,9,15,16]. The homogeneity of the foils and spatial expansion are important factors for this effect but are not the only cause. We used here a nickel sample irradiated on a 500 μm diameter area, in order to minimize these sources of error. We demonstrate that the calculations based on the UTA concept can give an absolute transmission different from what would be obtained for a collection of individual Doppler and Stark broadened lines, depending on the width of the lines and on their overlapping. A lowering of absorption due to the saturation of the strongest thin lines has been previously pointed out for low-Z elements [17,18]. This point is addressed here by calculating the spectra with statistically distributed individual lines in the ''resolved transition array'' (RTA) method [19,20].

The experimental arrangement is described in Sec. II. Section III explains the ion-by-ion SOSA description based on the UTA formalism. Given in Sec. IV, are the least-squares fits of the spectra obtained with the detailed SOSA calculation and comparison with the analysis done with the LTE superconfiguration (SCO) code [21] coupled with the radiative hydrodynamic code MULTI [22]. The very good fit obtained for the absolute value of the transmission with the RTA method is described in Sec. V.

II. EXPERIMENTAL SETUP AND DATA ACQUISITION

A gold cavity has been designed to heat sample foils with the neodymium laser energy available at the *Laboratoire pour l'Utilisation des Lasers Intenses* (LULI) facility. Two frequency-doubled beams ($\lambda = 0.53\,\mu$m) were focused on thin gold foils (100 nm thick) glued on 500 μm diameter holes, with an energy around 20 J each and a 600 ps pulse duration. The laser intensity was 5×10^{13} W/cm^2 in a 160 μm full width at half maximum (FWHM) focal spot size obtained by using random-phase plates. The rear x-ray emission of the foils was thermalized in a cylindrical cavity of 1 mm diameter and length as shown in Fig. 1. A nickel sample foil was glued on a 500 μm diameter hole [23]. Characterization of the cavity heating has been performed in previous experiments [24] and shows that the sample foil is heated by approximately 10% of the XUV energy emitted at the rear of one of the laser-irradiated gold foils. The radiation field in the cavity is very close to a 40 eV blackbody radiation field. The nickel sample was a 20 or 40 μg/cm^2 (225 or 450 Å) self-standing foil tamped by two coatings of 8 μg/cm^2 thick carbon (350 Å). Nickel was chosen because good thickness uniformity may be achieved with this element. The thickness of the absorber foil was measured with a quartz balance during deposition and optimized to provide a uniform volumetric heating. The foils were controlled with electronic microscope imaging that showed no holes or defects. Samples were fabricated in two different laboratories to check that the uncertainty on thickness had no influence on the transmission measurements. The absorption spectra were recorded with a thallium-hydrogen-phthalate (TIAP) flat crystal recording the 2-3 and 2-4 transitions of nickel in the range 12–14 Å (approximately 0.9–1.1 keV). A x-ray backlighter (BL) was obtained by tightly focusing a third laser beam ($\lambda = 0.53\,\mu$m) on a cesium iodine (CsI) flat target in order to get an intense continuum emission in the spectral range of interest. This beam was delayed by 500 ps with respect to the peak of the main beams, late enough to minimize the temperature variation and early enough to avoid the collision of the thin gold foils near the center of the cavity. The BL target was set at a distance of 4 mm from the cavity. This distance was large enough to neglect the heating of the sample by the BL source. The backlighter source was characterized on separate shots from the absorption measurement. Spectra were filtered by a 3 μm aluminum foil and recorded on Kodak DEF film. An additional 1.5 μm thick mylar filter and an aperture were set between the cavity and the spectrograph in order to limit the damage done to the TIAP crystal by the debris of the exploding gold cavity. The wavelength calibration was obtained by superimposing on the film an aluminum emission spectrum in second order and a CsI spectrum recorded with two successive laser shots without moving the spectrograph. An absolute wavelength error of 10 mÅ results from this method, and the instrumental broadening was measured on a thin aluminum line ($\lambda/\Delta\lambda = 700$). In this experiment, self-emission originating from the cavity was negligible. All the spectra have been corrected from film fog. Transmission was obtained by dividing the transmitted spectrum by the backlighter source spectrum, after subtracting the background from both spectra.

Different spectra have been recorded for 20 and 40 μg/cm^2 nickel foils. The hydrocode simulations that were run with the code MULTI [22] show that 20 or 40 μg/cm^2 foils are fairly homogeneously heated but that the temperature variations are not negligible during the measurement time. This is clearly seen in the calculations reported in Fig. 2. In this simulation, the sample is heated by 10% of the x-ray emission of the rear of a 100 nm gold foil, irradiated with 5×10^{13} W/cm^2 laser intensity at 0.53 μm wavelength, and the areal density of the sample is 40 μg/cm^2. The temperature of the foil is not very sensitive to its thickness, but is linked to the x-ray emission of the cavity, i.e., to the laser energy and alignment conditions. The spectra are very dependent on the ionization of the foil, which is governed by

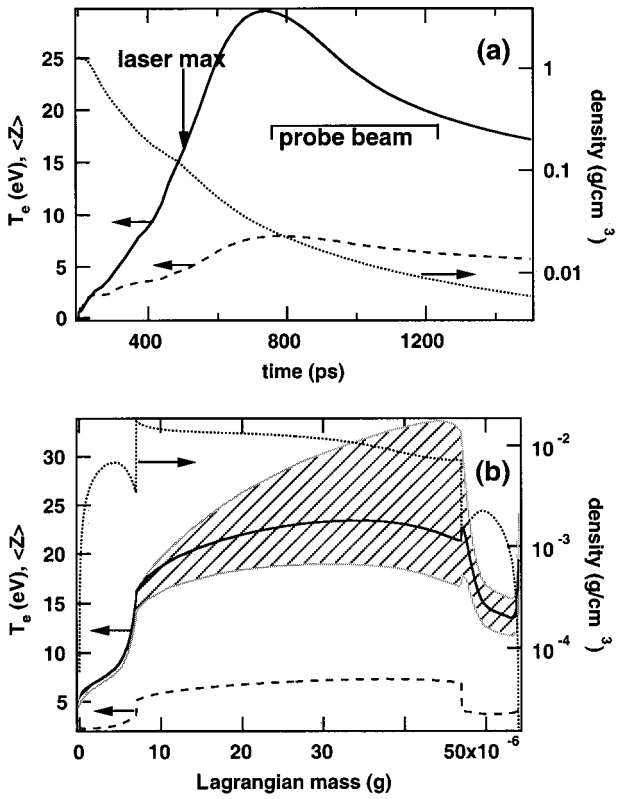

FIG. 2. Electron temperature, density, and average charge calculated by the hydrocode MULTI. Full line, temperature; dotted line, density; dashed line, average charge; (a) parameters at the center of the foil, as a function of time; the x-ray probe duration is shown; (b) parameters at time 1000 ps as a function of Lagrangian mass, proportional to the original position of the cells. The uncertainty due to time averaging is indicated on the temperature, the area between the curves traced at 1000 ± 300 ps is dashed. X-rays come from the right.

the heating of the foil and is more influenced by temperature variations than by density.

III. UTA FORMALISM FOR INDIVIDUAL IONS

The number of lines in the spectra is so large that, in a first attempt, the interpretation of the spectrum can be made using the UTA formalism [10]. Separate calculations of the Ni VI (Ni^{5+}) through Ni XII (Ni^{11+}) spectra lead to the identification of the different features of the experimental spectra.

First, the configurations of each ionic species involved in the transitions are selected. In the example of Ni VIII (21 electrons), the average energies of the 209 configurations belonging to the following complexes are computed, by means of the RELAC code [25]:

$$(1s)^2(2s2p)^8(3s3p3d)^{11},$$

$$(1s)^2(2s2p)^8(3s3p3d)^{10}(4s4p4d4f)^1,$$

$$(1s)^2(2s2p)^8(3s3p3d)^{10}(5s5p5d5f5g)^1.$$

Among these configurations, those whose average energies are less than 100 eV above the ground configuration are selected. Indeed, LTE is assumed inside a superconfiguration at a temperature around 20 eV, identical for all the ions. In this approximation, for $T_e = 20$ eV, a Boltzmann factor smaller than $\exp(-100/20) = 0.007$ would yield a negligible population. The upper configurations are selected among the 396 configurations belonging to

$$(1s)^2(2s2p)^7(3s3p3d)^{12},$$

$$(1s)^2(2s2p)^7(3s3p3d)^{11}(4s4p4d4f)^1,$$

$$(1s)^2(2s2p)^7(3s3p3d)^{11}(5s5p5d5f5g)^1.$$

They are introduced into the calculations if they give transition arrays with an average wavelength between 12 and 14.5 Å. Corresponding excitations are

$$2s\text{-}3p,4p,5p,$$

$$2p\text{-}4s,5s,$$

$$2p\text{-}3d,4d,5d.$$

The levels belonging to configurations with a hole in the $2p$ shell gather into relativistic subconfigurations corresponding to $2p_{1/2}$ and $2p_{3/2}$ holes, due to the large value of the spin-orbit integral ζ_{2p}. The arrays corresponding to the $2p$-nd excitation exhibit three peaks (subarrays): $2p_{1/2}$-$nd_{3/2}$, $2p_{3/2}$-$nd_{5/2}$ and $2p_{3/2}$-$nd_{3/2}$, which intensities, without configuration interaction, are proportional to 5, 9, and 1, respectively. The third peak may be neglected. The splitting between the main two peaks is about $3/2\ \zeta_{2p}$. In the example of Ni VIII, where $\zeta_{2p} = 91\,840\ \mathrm{cm}^{-1}$, this splitting is equal to $137\,760\ \mathrm{cm}^{-1}$, i.e., 17 eV. In the $2p$-ns cases, there are only two peaks. On the contrary, the $2s$-np arrays are not separated in subarrays. Consequently, except for the case $2s$-np, the spin-orbit-split array (SOSA) approach [13] has been used, taking into account the interaction between the relativistic subconfigurations with the method described in Ref. [14].

Presented in Fig. 3 are the transmission values calculated for each ionic species, without any scaling between the different ions. Populations inside superconfigurations are calculated assuming LTE at $T_e = 16$ eV. Transitions are identified as shown in the plot of Ni VII to Ni IX. The $2p$-$3d$ double-peaked structure due to the spin-orbit splitting shifts towards higher energy when the screening of the nucleus decreases. It has to be noted that, unlike the ionic balance, which is very sensitive to the temperature, the excitation balance and the transmissions calculated for each ion do not vary rapidly with the electron temperature. The changes in individual transmissions induced by a few eV temperature difference affect only slightly the transmission calculated for each ion. In consequence, an uncertainty of a few eV in the temperature used in the SOSA calculation does not change dramatically the ionic balance and the simulated x-ray spectra.

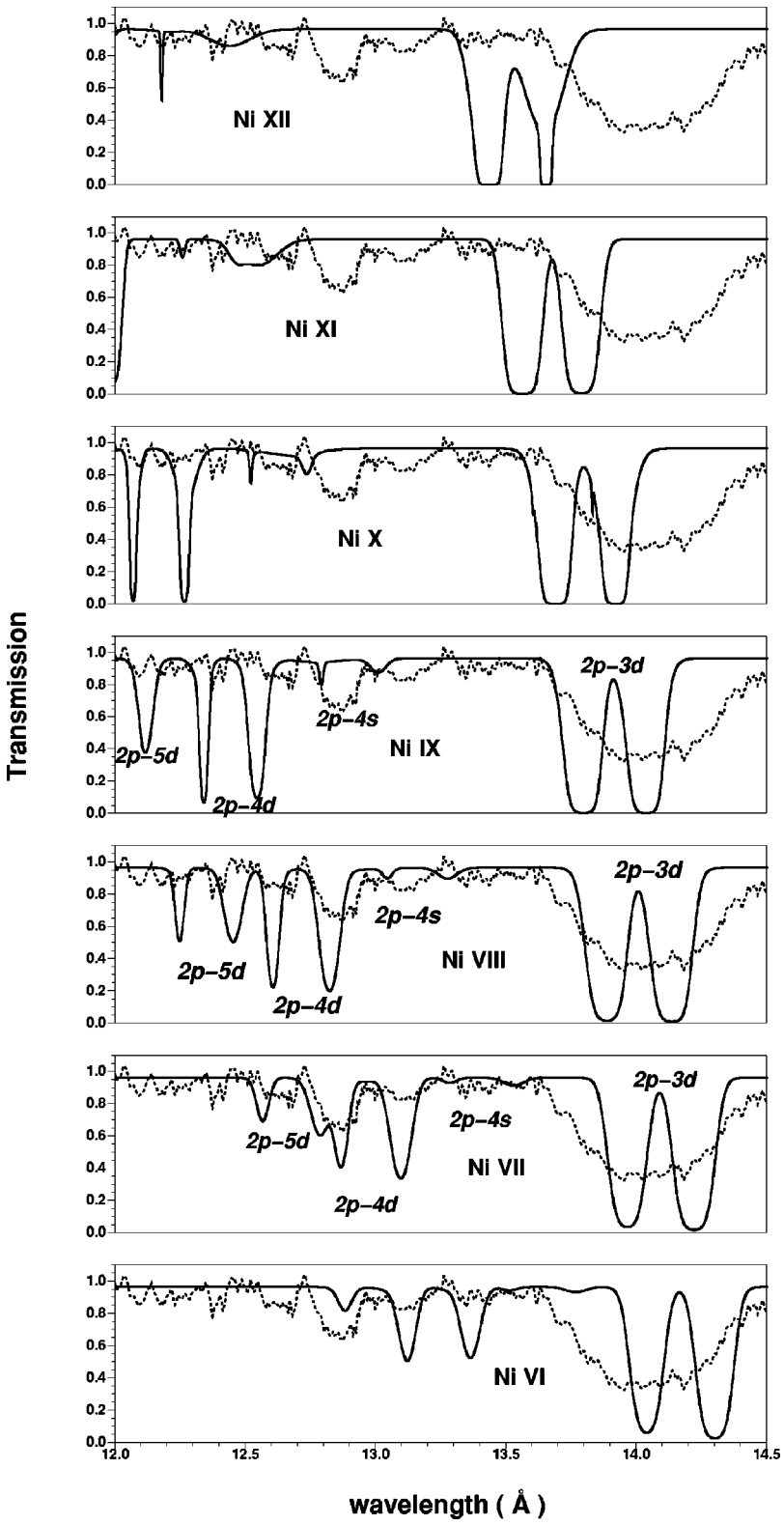

FIG. 3. Detailed SOSA formalism calculations showing the transmission calculated for each ionic species Ni VI to Ni XII for LTE at 16 eV assumed inside superconfigurations. The transitions are identified in the plot of the Ni VII to Ni IX absorption. The dashed curve is the experimental spectrum of Fig. 4 shown for comparison.

IV. ANALYSIS WITH SOSA CALCULATIONS

Comparisons between two experimental spectra and the calculations performed with the detailed SOSA method presented in Sec. III are shown for different parameters in Fig. 4 ($\rho l = 40\ \mu$g/cm^2, temperature inside superconfigurations $T_e = 16$ eV,) and Fig. 5 ($\rho l = 20\ \mu$g/cm^2, temperature inside superconfigurations $T_e = 20$ eV). The transmission t^{calc} is obtained from the mass absorption coefficients K_j calculated for each ion at a given temperature and reads

$$t^{\mathrm{calc}}(\lambda_k) = \exp - \left[\rho l \sum_{j=1}^{p} (f_j K_j(\lambda_k)) \right], \qquad (1)$$

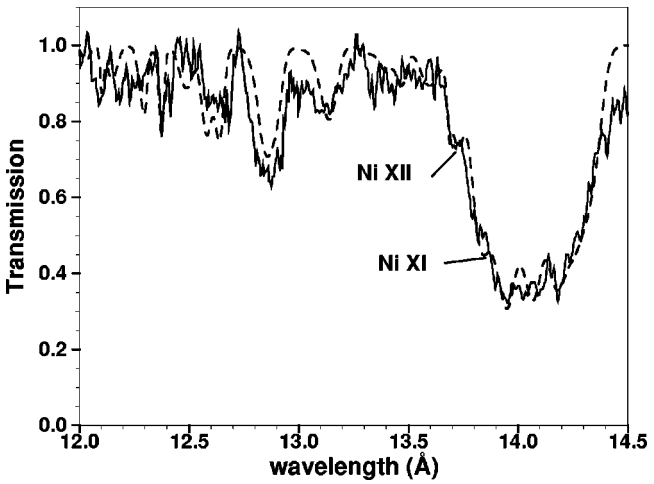

FIG. 4. Comparison of the experimental spectrum obtained for 40 μg/cm^2 of Ni (full line), with the detailed SOSA calculations (dashed line). The deduced ion distribution is given in Table I. The spectrum is simulated with an areal density of 28 μg/cm^2 and with LTE at 16 eV assumed inside superconfigurations.

where ρl is the areal mass density of the absorbing sample, f_j are the unknown ionic fractional populations of the p ions introduced in the calculation, and λ_k are the wavelengths of the $k=1,N$ points of the experimental spectrum. The following root-mean-square error has to be minimized:

$$\sqrt{\frac{1}{N}\sum_{k=1}^{N}\left\{\left(t^{\mathrm{expt}}(\lambda_k)-t^{\mathrm{calc}}(\lambda_k+\Delta\lambda)\right\}^2}, \qquad (2)$$

where t^{expt} and t^{calc} are the experimental and computed transmissions, calculated at each experimental point k. $\Delta\lambda$ is a small wavelength variation parameter introduced to take into account the systematic mismatch of wavelength calculated by RELAC and the uncertainty on the experimental wavelength determination. The areal density ρl, which rules the absolute value of the transmission has to be adjusted for a best fit, and not fixed at the nominal value as will be discussed later. The following two-steps procedure has been used to determine the set of variables $(f_j,\rho l,\Delta\lambda)$.

For fixed ρl and $\Delta\lambda$, (t^{expt}-t^{calc}) is minimized, inducing a linear least-squares system of N equations with p unknowns f_j $(p \ll N)$. The solution is saved and the root-mean-square error given by Eq. (2) is calculated if all the ionic fractions f_j are positive and their sum $\Sigma f_j \leqslant 1$ is compatible with the determined ionic composition. For example, in the 16 eV case, the ion distribution is such that the ion Ni V, which is not included in the calculation, is not negligible and could represent more than 5% of the total population. So, the sum Σf_j is assumed to be less than unity to take into account the fractions of neglected ions.

This process is performed for a grid of physically acceptable values of $(\rho l,\Delta\lambda)$. The best fit is the set $(f_j,\rho l,\Delta\lambda)$ which gives the minimum value of all the saved root-mean-square errors. Table I gives the ionic balance obtained for the two experimental cases. The temperature used to calculate the configuration distribution was 20 eV for the 20 μg/cm^2 case and 16 eV in the 40 μg/cm^2 case due to different experimental conditions. These temperatures were estimated from a comparison of the experimental data with LTE calculations performed with the superconfiguration code SCO, and from aluminum spectra measured in multilayered aluminum/nickel samples [21,26]. The Ni VIII ion was dominant for the two shots. The balance is changing between the highest and lowest ions when the heating conditions vary, five or six different species being significantly populated. The ion distribution is not much broader for 40 μg/cm^2 than for 20 μg/cm^2, showing that the spatial gradients do not increase with the foil thickness. In the different spectra, the contributions of Ni XI and Ni XII are very small, but, as the corresponding transition arrays appear on the side of the $2p$-$3d$ feature, they can be identified as shown in Fig. 4. It may be noted that they fit very well the experiment. These identified Ni XI and Ni XII structures permit to check that the wavelengths used in the theoretical spectra and the experimental calibration agree. The fit of Fig. 4 is remarkably good, not only for the $2p$-$3d$ structure around 14 Å, but also for the 2 to 4 transitions that are much weaker. It has to be noted that the experimental spectrum of Fig. 4 is better reproduced by the SOSA calculations done for an areal mass of 28 μg/cm^2 lower than the nominal values of 40 μg/cm^2. This discrepancy is also present in the case of the thinner foil for which a value of 14 μg/cm^2 was used instead of 20 μg/cm^2 (Fig. 5).

TABLE I. Ionic fractions and average charge determined by comparison of different experimental data with the detailed SOSA calculations. The 20 μg/cm^2 case has been fitted with the detailed SOSA method with LTE at 20 eV assumed inside superconfigurations. For the 40 μg/cm^2 case, the detailed SOSA were calculated with LTE at 16 eV assumed inside superconfigurations. In both case, the wavelength correction $\Delta\lambda$ was -36 mÅ.

	SOSA 20 (μg/cm^2)	SOSA 40 (μg/cm^2)
Ni VI (%)	7	14.8
Ni VII (%)	10.8	22.5
Ni VIII (%)	15.2	25.4
Ni IX (%)	18.6	13.7
Ni X (%)	16.3	4.4
Ni XI (%)	12.2	2.2
Ni XII (%)	4.65	1.0
$\langle Z\rangle$	7.9	6.8

We have found that the charge distribution obtained by fitting the spectra with the detailed SOSA method is broader than the LTE distribution given by SCO, where only three ion species are populated for a given set of density and temperature. This could be attributed to non-LTE effects or to the presence of gradients in the plasma. The hypothesis that the plasma is close to LTE was checked on data measured on aluminum and on mixtures of aluminum and nickel, in the same experimental conditions as in the present paper: the aluminum distribution follows well the LTE distribution [23,26]. We have also estimated the ratio β of radiative to collisional rates that is of the order of 10^{-3}, i.e., consistent

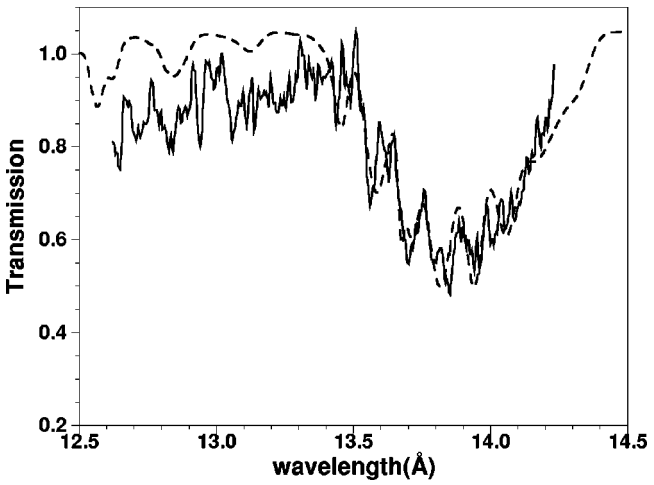

FIG. 5. Comparison of the experimental spectrum obtained for a 20 μg/cm^2 Ni foil (full line), with the detailed SOSA calculations (dashed line). The spectrum is simulated with an areal density of 14 μg/cm^2 and with LTE at 20 eV assumed inside superconfigurations.

with the LTE assumption. Temporal and spatial variations of the temperature could explain this broader distribution. We have calculated this gradient effect by coupling the SCO results to the hydrodynamic data given by the code MULTI. The code SCO is run for different sets of density and temperatures given by MULTI, and the obtained profiles are integrated in space and time, during 600 ps around a fixed measuring delay. Figure 6 shows the comparison of the experimental profile obtained for 40 μg/cm^2 (the same as in Fig. 4) with integrated profiles calculated with the SCO code for two delays of measurement (100 and 500 ps). The areal mass has been lowered to 28 μg/cm^2 as in the analysis with the SOSA method. The width and wavelength position of the $2p$-$3d$ structure are qualitatively well reproduced for the experimental measuring time $t=t_0+500$ ps. A better agreement is obtained with slightly steeper gradients as obtained earlier in time (see Fig. 6). We conclude that the ion distribution is broadened by temperature gradients, in accordance with the ion distribution, broader than an LTE one, obtained with the SOSA method.

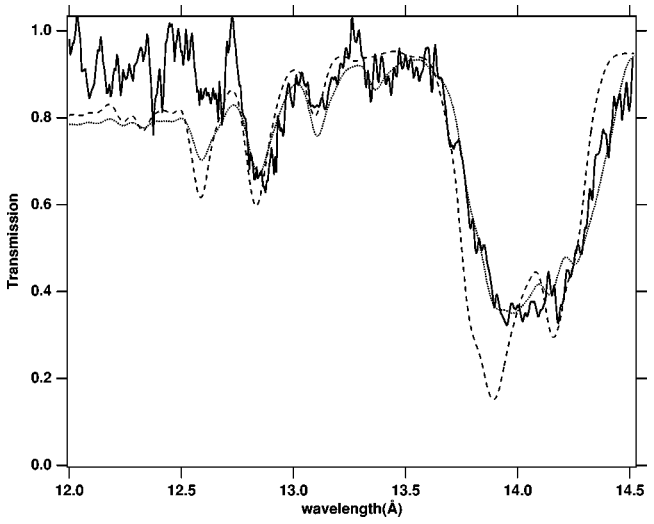

FIG. 6. Comparison of the experimental spectrum obtained for 40 μg/cm^2 of Ni (full line), with the spectra obtained by integrating the profiles calculated with the code SCO for sets of densities and temperatures, which follow the hydrodynamics of the plasma as given by the code MULTI. The profile integrated during 600 ps around the measuring time $t=t_0+500$ ps is represented as a thick-dashed line. The better agreement obtained for steeper gradients at time $t=t_0+100$ ps is plotted as a dotted line.

V. ANALYSIS WITH THE RTA FORMALISM

The Gaussian curves used in the UTA and SOSA models have proved to be adequate for the simulation of emission spectra, but this description of spectra by continuous functions may not be sufficient for the calculation of the plasma absorption. Indeed, the Rosseland opacity is very sensitive to the occurrence of gaps, i.e., separated lines, in the absorption coefficient $K(\nu)$. For this reason, the RTA statistical model [19] that introduces individual lines in the SOSA model has been used here in its improved version [20]. In that method, the energies E_1 and E_2 of the upper and lower levels of the lines obey Gaussian statistical distributions. Their variances are given by compact formulas in terms of the energy radial integrals. The line amplitudes obey a Poissonian distribution. Moreover, the energy and the amplitude distributions are correlated. This can be observed noticing that, on the average, the stronger lines lie closer to the average energy of the array than the weaker lines. After having obtained the parameters of the different distributions, the energies E_1 and E_2 are first picked at random for each line in the relevant Gaussian distributions. Then, the amplitude is picked at random in a Poisson distribution that depends on the values of E_1 and E_2. The Boltzmann factor is then introduced for the population of the level. As a result, the millions of lines of the recorded spectra are simulated statistically in a simple way. Let us recall that, in spite of the fact that each line is not calculated exactly, the model yields the following correct values:

(i) for the moments of the distribution of the unweighted and weighted line energies, and of the line strengths;

(ii) for the numbers of lines and their total strengths, in energy domains narrower than the width of a transition array.

This has been demonstrated by comparing, for different types of transition arrays, the theoretical spectra obtained by the Slater-Condon method (diagonalization of large matrices) and by the RTA simulation.

In the Ni spectrum, all the arrays introduced in the SOSA simulation (Sec. IV) have been simulated using the RTA method, except the six arrays corresponding to the excitations $2p-ns$, which are very weak and contain more than 400 000 lines. As an example, the 20 transition arrays considered in the case of Ni VI are listed in Table II. For each transition array, which is separated in relativistic subarrays, all the lines have been simulated (the number of lines of an array is calculated by means of a formula given in Ref. [27], with a 2% uncertainty). For Ni VI, the total number of lines is about 2 687 000. For the other ions, this number is lower

TABLE II. Transition arrays in Ni VI that have been simulated line-by-line in the RTA formalism.

Lower configuration	Upper configuration	Transition	Number of lines
$2s^2 2p^6 3s^2 3p^6 3d^5$	$2s^2 2p^5 3s^2 3p^6 3d^6$	$2p$-$3d$	2140
$2s^2 2p^6 3s^2 3p^6 3d^5$	$2s^2 2p^5 3s^2 3p^6 3d^5 4s$	$2p$-$4s$	7500
$2s^2 2p^6 3s^2 3p^6 3d^5$	$2s^2 2p^5 3s^2 3p^6 3d^5 4d$	$2p$-$4d$	20 200
$2s^2 2p^6 3s^2 3p^6 3d^5$	$2s^2 2p^5 3s^2 3p^6 3d^5 5s$	$2p$-$5s$	7500
$2s^2 2p^6 3s^2 3p^6 3d^5$	$2s^2 2p^5 3s^2 3p^6 3d^5 5d$	$2p$-$5d$	20 200
$2s^2 2p^6 3s^2 3p^6 3d^4 4s$	$2s^2 2p^5 3s^2 3p^6 3d^5 4s$	$2p$-$3d$	8200
$2s^2 2p^6 3s^2 3p^6 3d^4 4p$	$2s^2 2p^5 3s^2 3p^6 3d^5 4p$	$2p$-$3d$	65 200
$2s^2 2p^6 3s^2 3p^6 3d^4 4d$	$2s^2 2p^5 3s^2 3p^6 3d^5 4d$	$2p$-$3d$	144 300
$2s^2 2p^6 3s^2 3p^6 3d^4 5s$	$2s^2 2p^5 3s^2 3p^6 3d^5 5s$	$2p$-$3d$	8200
$2s^2 2p^6 3s^2 3p^5 3d^6$	$2s^2 2p^5 3s^2 3p^5 3d^7$	$2p$-$3d$	34 200
$2s^2 2p^6 3s^2 3p^5 3d^6$	$2s^2 2p^5 3s^2 3p^5 3d^6 4s$	$2p$-$4s$	167 500
$2s^2 2p^6 3s^2 3p^5 3d^6$	$2s^2 2p^5 3s^2 3p^5 3d^6 4d$	$2p$-$4d$	457 600
$2s^2 2p^6 3s^2 3p^5 3d^6$	$2s^2 2p^5 3s^2 3p^5 3d^6 5s$	$2p$-$5s$	167 500
$2s^2 2p^6 3s^2 3p^5 3d^6$	$2s^2 2p^5 3s^2 3p^5 3d^6 5d$	$2p$-$5d$	457 600
$2s^2 2p^6 3s^2 3p^6 3d^4 5p$	$2s^2 2p^5 3s^2 3p^6 3d^5 5p$	$2p$-$3d$	65 200
$2s^2 2p^6 3s^2 3p^6 3d^4 4f$	$2s^2 2p^5 3s^2 3p^6 3d^5 4f$	$2p$-$3d$	208 100
$2s^2 2p^6 3s^2 3p^6 3d^4 5d$	$2s^2 2p^5 3s^2 3p^6 3d^5 5d$	$2p$-$3d$	144 300
$2s^2 2p^6 3s^2 3p^6 3d^4 5f$	$2s^2 2p^5 3s^2 3p^6 3d^5 5f$	$2p$-$3d$	208 100
$2s^2 2p^6 3s^2 3p^6 3d^4 5g$	$2s^2 2p^5 3s^2 3p^6 3d^5 5g$	$2p$-$3d$	242 800
$2s^2 2p^6 3s^2 3p^5 3d^5 4s$	$2s^2 2p^5 3s^2 3p^5 3d^6 4s$	$2p$-$3d$	250 400

(for example, there are 506 000 lines in the Ni IX spectrum) and the total number is larger than 7 124 000 lines for the whole spectrum.

The next step is the introduction of the individual line width. As the evaluation of this width is not trivial, and as the number of lines is large, the same width was introduced for all the lines. Doppler broadening, for a 20 eV temperature, gives a Gaussian profile with a FWHM such that $\lambda/\Delta\lambda = 25\,000$. The Lorentzian width of the line is due to the natural and the autoionization widths and Stark broadening. The natural and autoionization widths have been estimated for different lines of the Ni VIII ion that is dominant in our experiment. The majority of the lines have rates of the order of magnitude of $10^{12}\,s^{-1}$, which gives a negligible width compared to the Doppler width. The Stark width has been evaluated taking into account the elastic [28] and inelastic [29] electron collisions, and the ion contribution [30]. The width of the $2p$-$3d$ line of Ni VIII has been calculated for $T_e = 20$ eV and different electron densities. Stark broadening starts to play a role for electron densities larger than $10^{21}\,cm^{-3}$, i.e., for densities much larger than the experimental ones. Following these evaluations, the RTA calculation has been performed using the ion distribution obtained by the SOSA method with a Gaussian width $\lambda/\Delta\lambda = 25\,000$, corresponding to a dominant Doppler width. The obtained transmission profile has been convolved with the $\lambda/\Delta\lambda = 700$ instrumental broadening.

In Fig. 7, shown is the result of the RTA calculation performed with the ion distribution given by the SOSA calculation. A remarkable agreement is obtained for the nominal areal density of 40 $\mu g/cm^2$. This was never obtained when the spectra were reproduced with the SOSA formalism (ion-by-ion SOSA or the SCO code) [14,21]. The same agreement has been obtained for the 20 $\mu g/cm^2$ shot, for the same width of the individual lines ($\lambda/\Delta\lambda = 25\,000$). Additionally, we have performed the same calculation with different areal masses ($\rho l = 30$ and 50 $\mu g/cm^2$), and with different Gaussian widths ($\lambda/\Delta\lambda = 10\,000$ and 50 000). In these four cases, the convolved transmission profiles were noticeably different from the experimental one.

This is due to the well-known effect of saturation of individual lines [17,18]; if an individual narrow line is absorbing

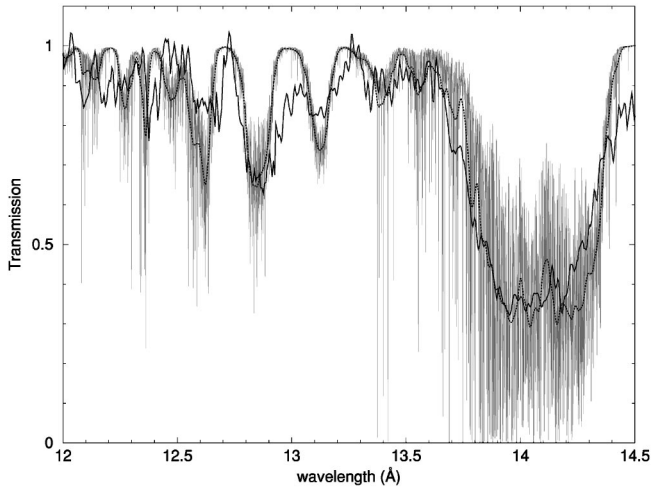

FIG. 7. Comparison of the experimental spectrum of Fig. 4 (full thick line), obtained for 40 $\mu g/cm^2$ of Ni, with the RTA calculations. Full gray thin line, individual line (RTA) calculation done for an areal density of 40 $\mu g/cm^2$, with the ionic distribution given by the detailed SOSA calculation (see Table I, column 2); dotted line, RTA profile convolved with the instrumental profile ($\Delta E = 1.26$ eV, i.e., $\lambda/\Delta\lambda = 700$).

so much that its transmission is saturated, its total absorption integrated on the line profile is lowered, i.e., its transmission is higher. This effect is obvious when the individual line transmission falls to zero. However, it starts to play a role even if the individual line transmission does not reach zero. The nonconvolved profile calculated with the RTA formalism plotted in Fig. 7 exhibit a number of very low transmission and saturated individual lines. This explains why the profile convolved by the instrumental broadening gives a higher transmission than in a nonsaturated case. This result shows that the transmission calculated with the UTA or the SOSA approaches is too low, when the individual lines are narrow and their absorption is saturated. Indeed, these lines contribute too much to the absorption if they are part of a transition array, because the saturation effect cannot be taken into account.

We have compared the Planck and Rosseland opacities calculated with the SOSA and the RTA methods, in the energy range of the experiment (860 to 1085 eV). As expected, the Planck opacities are identical due to the conservation of the area limited by the opacity profile. The Rosseland opacity, calculated with the SOSA formalism is notably larger than the value obtained in the RTA case, due to the gaps between narrow lines.

VI. CONCLUSION

The present analysis of the absorption of the $2p$-$3d$ and $2p$-$4d$ transitions in nickel brings very complementary conclusions to what had been measured in iron [6]. An analysis based on a least-squares fit of the experimental absorption with detailed SOSA calculations performed ion by ion enables the determination of the ion distribution of heated medium-Z elements, without assuming that the ions are in LTE. The ion distribution obtained with this method is broader than an LTE distribution due to temporal and spatial variations of the temperature, as demonstrated by calculations performed with the code SCO coupled with the hydrodynamic code MULTI.

An important point raised in this paper is the use of the RTA formalism to overcome the discrepancy between experiments and simulations concerning the areal density found in a number of studies. When the line profiles are narrow and the instrumental broadening is large, the absorption coefficients calculations based on the UTA formalism average the individual lines, and their saturation is artificially masked. The line-by-line calculations like OPAL [3,4] and HULLAC [31], and the RTA formalism [20] are the only methods that may reproduce the experimental spectra with the nominal areal mass, when saturation of the individual lines plays a role. The evaluation of the line widths remains a crucial problem for reliable calculations of the absolute value of the transmission.

ACKNOWLEDGMENTS

The authors want to thank O. Peyrusse for providing Stark broadening calculations. They acknowledge the support of the technical staff of LULI, in particular R. Konig. The nickel foils have been made in the Institut de Physique Nucléaire at Paris-Sud University and in the University of Munich. The summation of the line profiles in the RTA method has been performed on the massively parallel computer T3E at IDRIS (Computer Center of the Center National de la Recherche Scientifique, at Orsay). This work was supported by the European Community, through Contract No. FMGECT950044 of the Large-Scale Facility ''Training and Mobility of Researchers Program.'' One of us (M.F.) was financed by Contract No. Praxis XXI/BD/13732/97.

[1] S. Turck-Chièze, S. Basu, A. S. Brun, J. Christensen-Dalsgaard, A. Eff-Darwich, I. Lopes, F. Pérez-Hernandez, G. Berthomieu, J. Provost, R. K. Ulrich, F. Baudin, P. Boumier, J. Charra, A. H. Gabriel, R. A. Garcia, G. Grec, C. Renaud, J. M. Robillot, and T. Roca Cortès, T. Sol. Phys. **175**, 247 (1997).

[2] L. B. Da Silva, B. J. Mac Gowan, D. R. Kania, B. A. Hammel, C. A. Back, E. Hsieh, R. Doyas, C. A. Iglesias, F. J. Rogers, and R. W. Lee, Phys. Rev. Lett. **69**, 438 (1992).

[3] F. J. Rogers and C. A. Iglesias, Astrophys. J., Suppl. Ser. **79**, 507 (1992).

[4] F. J. Rogers and C. A. Iglesias, Science **263**, 50 (1994).

[5] A. Gautschy and H. Saio, Annu. Rev. Astron. Astrophys. **33**, 75 (1995).

[6] C. Chenais-Popovics, H. Merdji, T. Mißalla, F. Gilleron, J. C. Gauthier, T. Blenski, F. Perrot, M. Klapisch, C. Bauche-Arnoult, J. Bauche, A. Bachelier, and K. Eidmann, Astrophys. J., Suppl. Ser. **127**, 275 (2000).

[7] M. Sako, S. M. Kahn, E. Behar, J. S. Kaastra, A. C. Brinkman, Th. Boller, E. M. Puchnarewicz, R. Starling, D. A. Liedahl, J. Clavel, and M. Santos-Lleo, Astron. Astrophys. **365L**, 168 (2001).

[8] P. T. Springer, K. L. Wong, C. A. Iglesias, J. H. Hammer, J. L. Porter, A. Toor, W. H. Goldstein, B. G. Wilson, F. J. Rogers, C. Deeney, D. S. Dearborn, C. Bruns, J. Emig, and R. E. Stewart, J. Quant. Spectrosc. Radiat. Transf. **58**, 927 (1997).

[9] T. S. Perry, K. S. Budil, R. Cauble, R. A. Ward, D. R. Bach, C. A. Iglesias, B. G. Wilson, J. K. Nash, C. C. Smith, J. M. Forster, S. J. Davidson, F. J. D. Serduke, J. D. Kilkenny, and R. W. Lee, J. Quant. Spectrosc. Radiat. Transf. **54**, 317 (1995).

[10] J. Bauche and C. Bauche-Arnoult, in *Laser Interactions with Atoms, Solids and Plasmas*, edited by R. M. More (Plenum Press, New York, 1994).

[11] T. S. Perry, P. T. Springer, D. F. Fields, D. R. Bach, J. D. Serduke, C. A. Iglesias, F. R. Rogers, J. K. Nash, M. H. Chen, B. G. Wilson, W. H. Goldstein, B. Rozsnyai, R. A. Waed, J. D. Kilkenny, R. Doyas, L. B. Da Silva, C. A. Back, R. Cauble, S. J. Davidson, J. M. Foster, C. C. Smith, A. Bar-Shalom, and R. W. Lee, Phys. Rev. E **54**, 5617 (1996).

[12] C. A. Iglesias, B. G. Wilson, F. J. Rogers, W. H. Goldstein, A. Bar-Shalom, and J. Oreg, Astrophys. J. **445**, 855 (1995).

[13] C. Bauche-Arnoult, J. Bauche, and M. Klapisch, Phys. Rev. A **31**, 2248 (1985).

[14] J. Bauche, C. Bauche-Arnoult, and M. Klapisch, J. Phys. B **24**, 1 (1991).
[15] C. A. Back, T. S. Perry, D. R. Bach, B. G. Wilson, C. A. Iglesias, O. L. Landen, S. J. Davidson, and B. J. B. Crowley, J. Quant. Spectrosc. Radiat. Transf. **58**, 415 (1997).
[16] H. Merdji, T. Mißalla, T. Blenski, F. Perrot, J. C. Gauthier, K. Eidmann, and C. Chenais-Popovics, Phys. Rev. E **57**, 1042 (1998).
[17] C. Chenais-Popovics, C. Fievet, J. P. Geindre, J. C. Gauthier, and I. Matsushima, Phys. Rev. A **42**, 4788 (1990).
[18] S. J. Davidson, C. L. S. Lewis, D. O'Neill, S. J. Rose, J. M. Foster, and C. C. Smith, in *Laser Interaction with Matter Proceedings*, Madrid 1988, edited by G. Velarde, E. Minguez, and J. M. Perlado (World Scientific, Singapore, 1989), p. 163.
[19] J. Bauche, C. Bauche-Arnoult, J. F. Wyart, P. Duffy, and M. Klapisch, Phys. Rev. A **44**, 5707 (1991); P. Duffy, M. Klapisch, J. Bauche, and C. Bauche-Arnoult, Phys. Rev. A **44**, 5715 (1991).
[20] J. Bauche and C. Bauche-Arnoult, Phys. Scr. T **65**, 99 (1996).
[21] T. Blenski, A. Grimaldi, and F. Perrot, Phys. Rev. E **55**, R4889 (1997).
[22] R. Ramis, R. F. Schmalz, and J. Meyer-ter-Vehn, Comput. Phys. Commun. **49**, 475 (1988); A. Mirone, J. C. Gauthier, F. Gilleron, and C. Chenais-Popovics, J. Quant. Spectrosc. Radiat. Transf. **58**, 791 (1997).
[23] C. Chenais-Popovics, F. Gilleron, M. Fajardo, H. Merdji, T. Mißalla, J. C. Gauthier, P. Renaudin, S. Gary, J. Bruneau, F. Perrot, T. Blenski, W. Fölsner, and K. Eidmann, J. Quant. Spectrosc. Radiat. Transf. **65**, 117 (2000).
[24] F. Gilleron, H. Merdji, M. Fajardo, O. Henrot, J. C. Gauthier, C. Chenais-Popovics, W. Fölsner, and K. Eidmann, J. Quant. Spectrosc. Radiat. Transf. **69**, 217 (2001); F. Gilleron, Doctorat thesis, Ecole Polytechnique, 2000.
[25] E. Koenig, Physica (Amsterdam) **62**, 393 (1972).
[26] C. Chenais-Popovics, M. Fajardo, J. C. Gauthier, K. Eidmann, W. Fölsner, F. Thais, T. Blenski, and F. Perrot, J. Quant. Spectrosc. Radiat. Transf. **71**249 (2001).
[27] J. Bauche and C. Bauche-Arnoult, J. Phys. B **20**, 1659 (1987).
[28] H. R. Griem, in *Plasma Spectroscopy* (MacGraw Hill, New York, 1964).
[29] M. S. Dimitrijevic and N. Konjevic, J. Quant. Spectrosc. Radiat. Transf. **24**, 451 (1980); M. S. Dimitrijevic and N. Konjevic, Astron. Astrophys. **163**, 297 (1986); M. S. Dimitrijevic and N. Konjevic, *ibid.* **172**, 345 (1987).
[30] B. Rozsnyai, J. Quant. Spectrosc. Radiat. Transf. **17**, 77 (1977).
[31] M. Klapisch, J. L. Schwob, B. S. Fraenkel, and J. Oreg, J. Opt. Soc. Am. **67**, 148 (1977).